JOURNAL OF APPLIED ELECTROCHEMISTRY 25 (1995) 729–739

Effect of state of charge on impedance spectrum of sealed cells
Part II: Lead acid batteries

V. V. VISWANATHAN*‡, A. J. SALKIND‡§, J. J. KELLEY‡§, J. B. OCKERMAN§

Department of Chemical Engineering, Rutgers University, Piscataway, NJ, 08855, USA‡ and UMDNJ-Robert Wood Johnson Medical School, Bioengineering Section, 675 Hoes Lane, Piscataway, NJ, 08854, USA§

Received 7 Feburary 1994; revised 20 October 1994

Alternating current impedance spectroscopy (ACIS) was performed on commercial sealed lead acid batteries. A method previously developed in the literature was modified to determine the state of charge of sealed lead acid cells by obtaining the impedance spectrum in a wide frequency range. The data were sensitive to state of charge at low frequencies. A modified Randles' circuit was used to fit the impedance data. The effect of the state of charge on the equivalent circuit parameters was determined.

List of symbols

R_Ω	ohmic resistance of battery (Ω)
C_{dl}	double layer capacitance (F)
Q_1	constant phase element representing double layer capacitance
Q_2	constant phase element representing Warburg diffusion
O	finite diffusion element
R_t	charge transfer resistance (Ω)
R_S, R_p	equivalent series and parallel resistance (Ω)
C_S, C_p	equivalent series and parallel capacitance (F)

1. Introduction

Impedance spectroscopy has been used to study both single electrodes [1–3] and cells [4–8] for lead acid batteries. Casson *et al.* [1] determined the charge transfer resistance and computed the magnitude of the exchange current density for lead dioxide electrodes to be equal to $0.24\,A\,m^{-2}$. They also studied the effects of porosity on the impedance spectrum, and concluded that the inductive behaviour was due to the porous nature of the electrodes. Hampson *et al.* [2, 3] measured the impedance of lead dioxide formed on lead and various lead alloys. They obtained an inductive loop with antimony as an alloying agent, thus showing that antimony facilitates a porous deposit of lead dioxide.

Driscoll and Szpak [4] used a.c. impedance measurements to detect defects in dry lead acid cells. Existence of an internal short gave rise to deviation of the slope of the Bode plot from −1 to 0 at low frequencies. Jindra *et al.* [5] measured the impedance of sealed lead acid cells and that of the individual electrodes during galvanostatic charging. They found that the positive electrode dominated the ohmic resistance of the sealed lead acid cell. The cell impedance at 0.1 Hz increased significantly with an increase in internal pressure during overcharge. This was useful in indicating the fully charged state of the cell. Hughes *et al.* [6] used impedance measurements to determine the state of charge of sealed lead acid cells. They found that the product of the charge transfer resistance and double layer capacitance increased exponentially with state of charge. In the case of lead acid batteries, the electrolyte participates in the reaction. Hence the ohmic resistance is expected to be a function of the state of charge of the battery. Barton *et al.* [7] found that the ohmic resistance decreased with increase in state of charge, consistent with the change in specific gravity of the electrolyte. Gopikanth and Sathyanarayana [8] determined the effect of state of charge on phase angle (ϕ), C_s and C_p, where C_s and C_p are equivalent series and parallel capacitance of the battery. They found that C_p and ϕ passed through a minimum, while C_S passed through a maximum as a function of state of charge. The study was carried out in the frequency range 10–100 Hz. Since the impedance parameters are most sensitive to state of charge at low frequencies, the above parameters were determined at frequencies ranging from 0.01–25 Hz in this work. An attempt has also been made to correlate the equivalent circuit parameters with the state of charge.

2. Experimental procedure

The lead acid batteries tested were: two 4 V 3 Ah batteries made by the Japan Storage Battery Company labelled M3 and M6; two 4 V 9 Ah

* Present address: Battelle Memorial Institute, Electrochemical Technology Group, 505 King Avenue, Columbus, Ohio 43201.

0021-891X

Table 1. Effect of state of charge on imaginary component Z'' (Ω) at various frequencies for lead acid battery M3

	Imaginary component Z'' (Ω)							
SOC/%	0.01 Hz	0.026 Hz	0.058 Hz	0.118 Hz	0.226 Hz	0.9 Hz	2.1 Hz	5.9 Hz
0	0.1134	0.0585	0.0646	0.0456	0.0442	0.0268	0.0282	0.0276
20	0.0808	0.0538	0.0501	0.0384	0.0343	0.0200	0.0195	0.0182
60	0.0848	0.0601	0.0490	0.0360	0.0286	0.0155	0.0132	0.0110
80	0.1186	0.0772	0.0519	0.0362	0.0280	0.0185	0.0163	0.0141
100	0.1514	0.0856	0.0535	0.0359	0.0281	0.0200	0.0193	0.0175

batteries also made by the Japan Storage Battery Company labelled N7 and N8; 6 V 6.5 Ah battery made by the Eagle Picher Battery Company labelled E1. The batteries were cycled by charging at the $C/4$ rate for 5 h, resting for 1 h and discharging at the $C/5$ rate using a cutoff voltage of 1.7 V/cell, where C is the nominal capacity of the battery. After a few cycles, impedance measurements were performed on the batteries at various states of charge (SOC). Impedance spectra were obtained for the cells at 0, 20, 40, 60 and 100% state of charge. The measurements were first made with the cells in the fully discharged state. After obtaining the spectrum at 0% SOC, the battery was charged at $C/5$ rate for 1 h. The impedance spectrum was obtained after 8 h on open circuit. The cell was subsequently discharged to determine its actual state of charge during the impedance measurement. This process was repeated till the data at 100% state of charge were obtained. The details of the experimental procedure and equivalent circuit analysis using Boukamp's software [9] are given in Part I of this paper [10].

3. Results and discussion

3.1. *Impedance data*

Figure 1 shows the Nyquist plot for battery N7 at 0% state of charge in the frequency range 0.01–631 Hz. The inductive points have not been plotted. There is a depressed semicircle at high frequency, while at low frequency, Warburg diffusion is observed.

3.2. *State of charge determination*

The imaginary components of the impedance at various states of charge at fixed frequencies are presented in Tables 1 and 2 for batteries M3 and M6. (Since the ohmic resistance forms a substantial portion of the real component of impedance, it masks the real component of the electrode impedance. Hence only the imaginary component has been presented.) The imaginary component of the impedance (Z'') goes through a minimum for the cells in the frequency range tested. Hence, the state of charge cannot be determined from the value of the imaginary component at a fixed frequency.

Gopikanth and Sathyanarayana [8] determined the effect of state of charge on ϕ, C_S and C_p in the frequency range 10–100 Hz, where C_S and C_p are the equivalent series and parallel capacitance respectively of the cell. Expressions for C_S and C_p were presented in Part I of this paper. In this work, it was observed that the above parameters were more sensitive to state of charge at low frequencies.

Figures 2–8 show the data for C_S, C_p and ϕ for lead acid batteries. Figure 2 shows that C_S goes through a maximum as a function of state of charge. Hence, the state of charge cannot be determined. It is also clear that C_S is more sensitive to state of charge at low frequency. C_S is approximately seven times higher at low frequency than the corresponding value at high frequency. Gopikanth and Sathyanarayana [8] found that ϕ passed through a minimum for lead acid batteries in the medium frequency range (10–100 Hz). Hence determination of state of charge was not possible. Figure 3 shows the dependence of ϕ on state of charge for battery M6. The phase angle ϕ goes through a minimum at 2.1, 5.9 and 25 Hz. At low frequencies, ϕ increases with state of charge, thus enabling the determination of state of charge. This figure clearly demonstrates the advantage of obtaining impedance spectra in a wide frequency range.

Table 2. Effect of state of charge on imaginary component Z'' (Ω) at various frequencies for lead acid battery M6

	Imaginary component Z'' (Ω)							
SOC/%	*0.01 Hz*	*0.026 Hz*	*0.058 Hz*	*0.118 Hz*	*0.226 Hz*	*0.9 Hz*	*2.1 Hz*	*5.9 Hz*
0	0.1100	0.0639	0.0655	0.0486	0.0461	0.0343	0.0362	0.0330
20	0.0834	0.0568	0.0485	0.0373	0.0321	0.0219	0.0202	0.0184
40	0.0777	0.0553	0.0430	0.0315	0.0249	0.0150	0.0130	0.0115
60	0.0873	0.0627	0.0462	0.0339	0.0263	0.0158	0.0129	0.0106
80	0.0758	0.0725	0.0483	0.0358	0.0253	0.0174	0.0156	0.0125
100	0.1506	0.0832	0.0505	0.0342	0.0258	0.0187	0.0176	0.0154

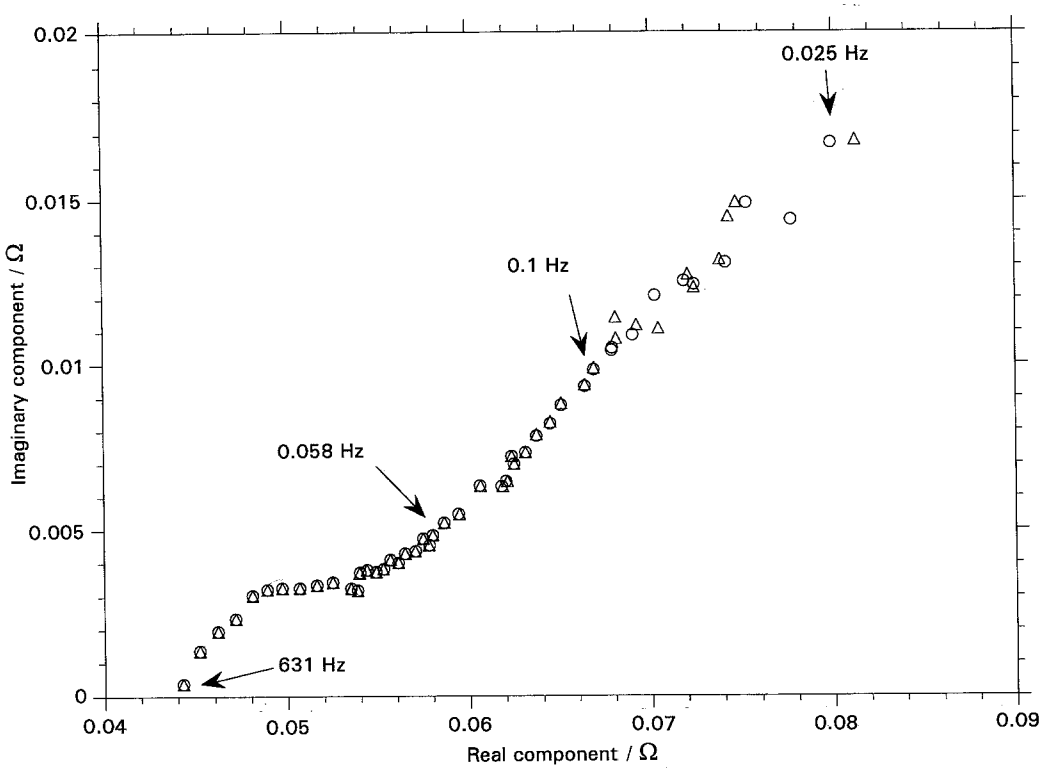

Fig. 1. Experimental (○) and calculated (△) impedance spectrum (Nyquist plot) for battery N7 at 0% state of charge in the frequency range 0.01–631 Hz.

Figure 4 shows that ϕ increases with state of charge at low frequency for batteries M3 and M6, while Fig. 5 shows that C_p increases with state of charge at the same frequencies for the above two batteries. For batteries N7 and N8, C_S decreases with state of charge at low frequencies (Fig. 6), while C_p increases with state of charge in the 0.9–5.9 Hz range (Fig. 7). Figure 8 shows that ϕ increases with state of charge in the 0.9–5.9 Hz range for battery E1. Hence, the state of charge of the batteries can be determined from Figs 4–8.

From the above results, it is evident that extensive tabulation of ϕ, C_s and C_p should be done at various states of charge at all frequencies. At certain frequencies, the above parameters pass through a maximum or minimum, thus making it difficult to determine the state of charge of the battery. At other

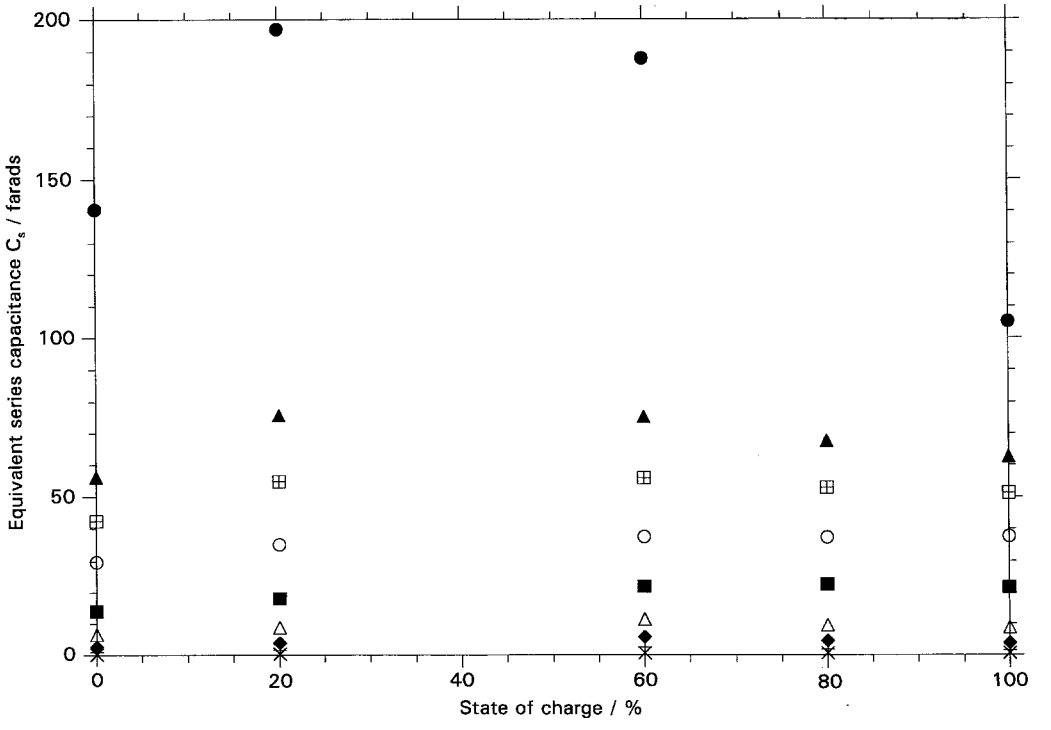

Fig. 2. Effect of state of charge on equivalent series capacitance C_s at various frequencies for battery M3. C_s passes through a maximum. Key: (●) 0.001, (▲) 0.034, (⊞) 0.058, (○) 0.118, (■) 0.300, (△) 0.900, (◆) 2.100, (+) 5.900 and (×) 25.1 Hz.

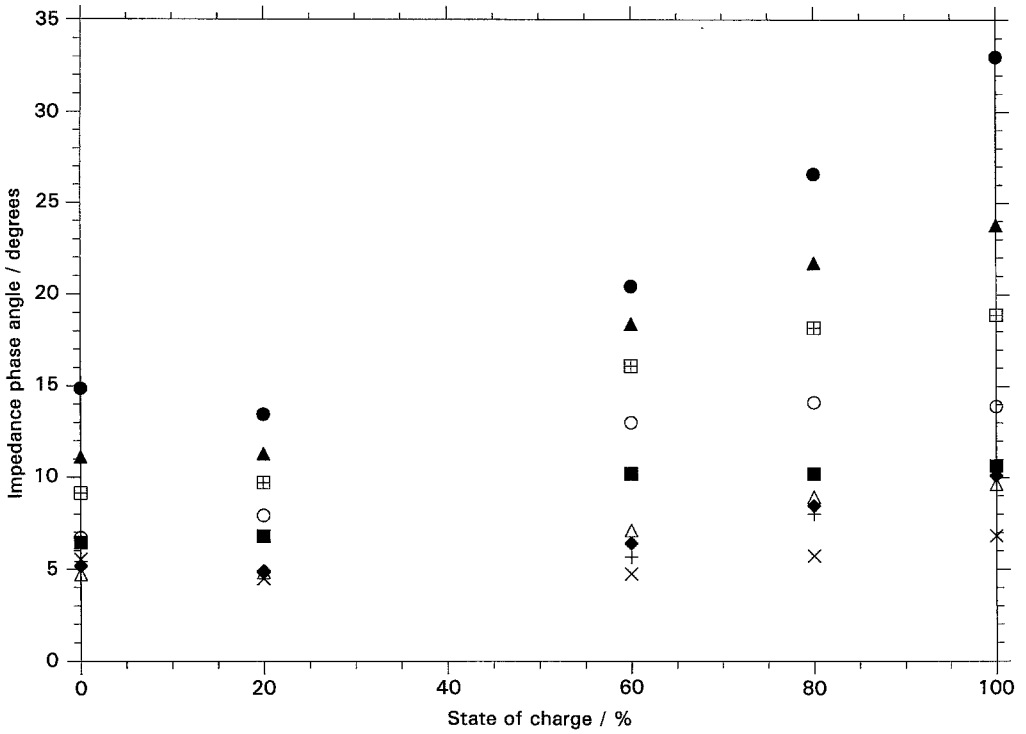

Fig. 3. Effect of state of charge on impedance phase angle at various frequencies for battery M3. The phase angle increases with increase in state of charge. Key: (●) 0.001, (▲) 0.034, (⊞) 0.058, (○) 0.118, (■) 0.300, (△) 0.900, (◆) 2.100, (+) 5.900 and (×) 25.1 Hz.

frequencies, one or more of the above parameters increase or decrease with state of charge, thus enabling determination of SOC.

The data for each battery type (M3, M6, N7 and N8) are close to each other. As discussed above, separate criteria should be set for each battery type to determine the state of charge. These criteria are the dependence of phase angle, C_s or C_p on state of charge at a fixed frequency. The relevant plots for each battery should be obtained separately and used to determine its state of charge.

3.3. *Equivalent circuit results*

The modified Randles' circuit $R_\Omega(Q_1(R_tQ_2))$ to which the data was fitted was described in Part I of this paper

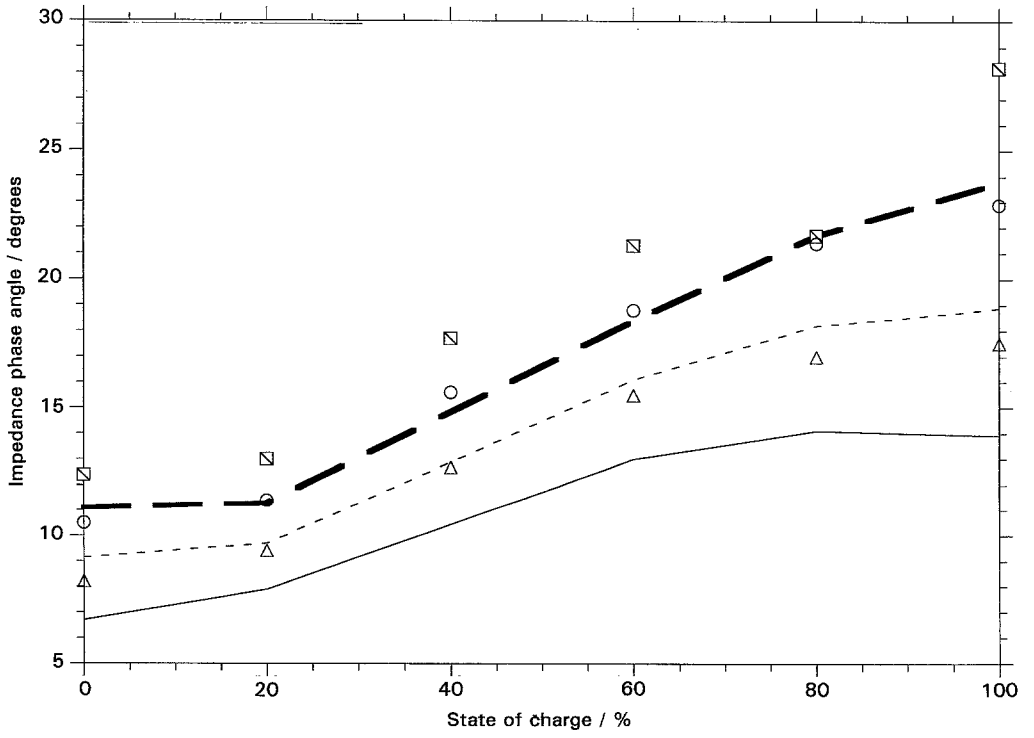

Fig. 4. Effect of state of charge on impedance phase angle for batteries M3 and M6 at low frequencies. The phase angle increases with state of charge for both batteries at the frequencies shown. For M3: (——) 0.003, (– – –) 0.058 and (——) 0.118 Hz; for M6: (□) 0.003, (○) 0.058 and (△) 0.118 Hz.

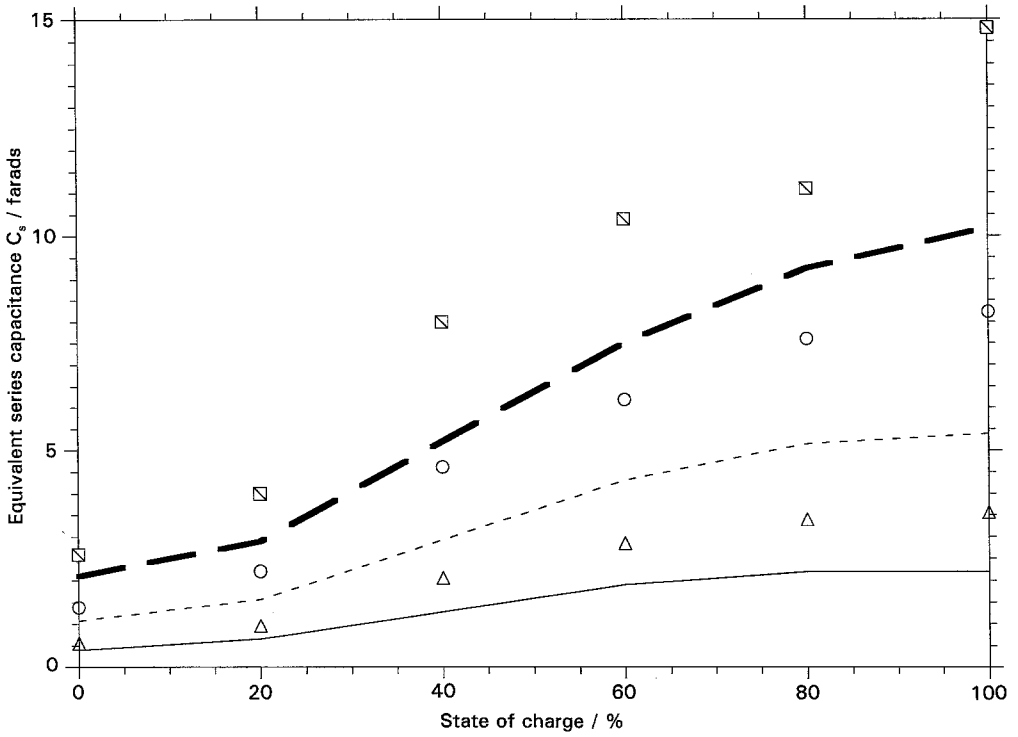

Fig. 5. Effect of state of charge on equivalent parallel capacitance C_p for batteries M3 and M6 at low frequencies. C_p increases with increase in state of charge. For M3: (——) 0.034, (– – –) 0.058 and (——) 0.118 Hz; for M6: (▨) 0.034, (○) 0.058 and (△) 0.118 Hz.

[10]. R_Ω is the ohmic resistance, Q_1 is the constant phase element representing double layer capacitance, R_t is the charge transfer resistance and Q_2 is the constant phase element corresponding to the Warburg element. Keddam *et al.* [11] modelled the inductive portion by a parallel (RL) combination in series with the modified Randles' circuit. They found that the values of R and L were not a function of the state of charge of the battery. Hence they concluded that inductive behaviour depended on the geometry of the system. Casson, Hampson and Williams [1] observed inductive behaviour for porous lead dioxide electrodes. They did not observe this for planar electrodes. They found that passivation of

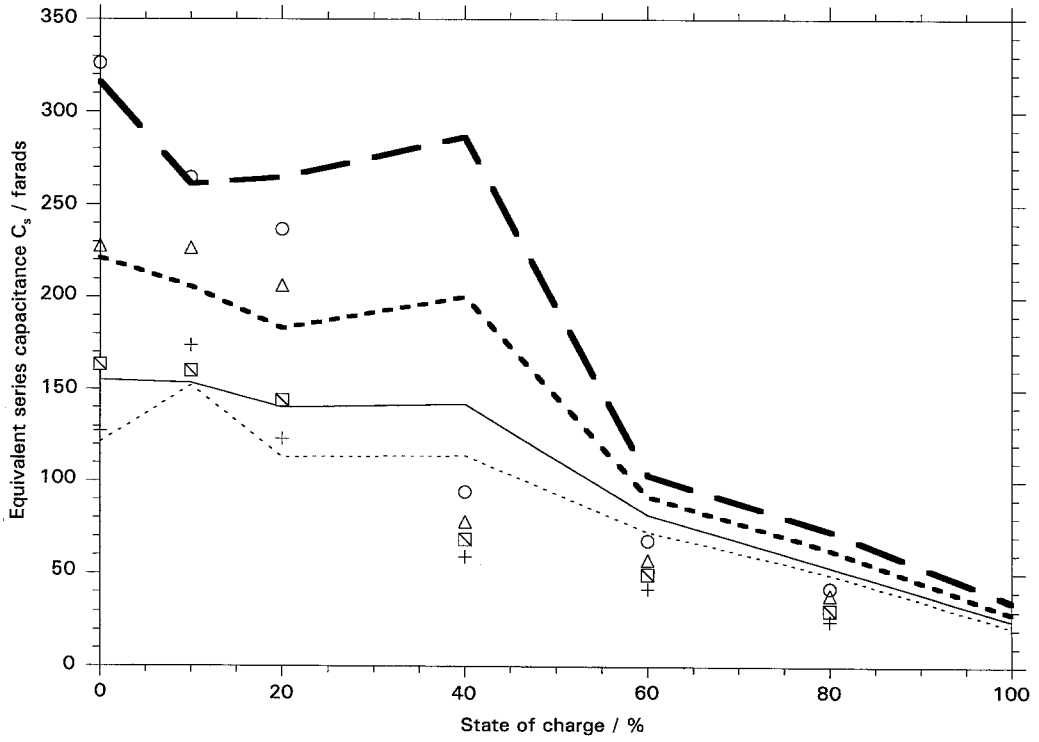

Fig. 6. Effect of state of charge on equivalent series capacitance C_s for batteries N7 and N8 at low frequencies. C_s decreases with increase in state of charge. For N7: (——) 0.034, (– – –) 0.058, (——) 0.082 and (· · · · · ·) 0.118 Hz; for N8: (○) 0.034, (△) 0.058, (▨) 0.082 and (+) 0.118 Hz.

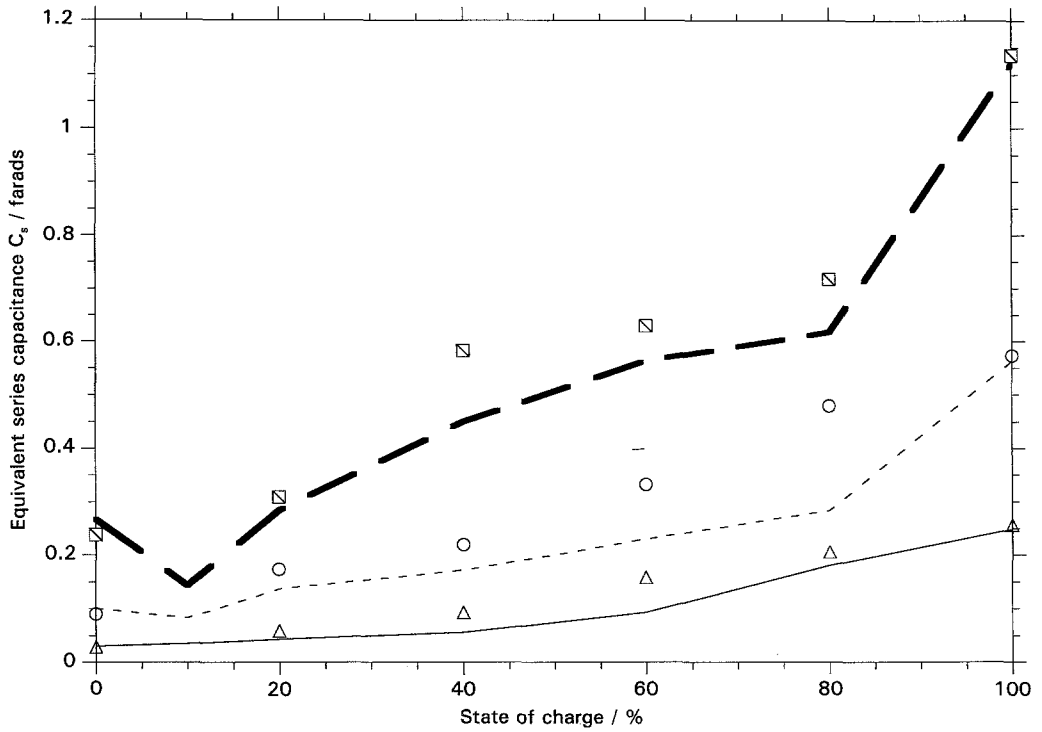

Fig. 7. Effect of state of charge on equivalent parallel capacitance C_p for batteries N7 and N8. C_p increases with state of charge. For N7: (——) 0.9, (– – –) 2.1 and (——) 5.9 Hz; for N8: (⊠) 0.9, (○) 2.1 and (△) 5.9 Hz.

the electrodes at 700 mV vs the $Hg/HgSO_4$ reference electrode eliminated the inductive behaviour. Since passivation leads to coverage of the pores, they concluded that the porosity of the electrodes was responsible for the inductive behaviour.

Table 3 gives the values of (RL) for some batteries. It is seen that inductance L depends on the type of battery. Hence there could be some geometry effects. These parameters were not determined for all states of charge. But the effect of state of charge on the inductance was determined qualitatively by noting the upper frequency limit for noninductive behaviour. The results are given in Table 4. This upper frequency limit decreased with increase in state of charge for each battery. Hence, it is possible that the inductive behaviour is determined

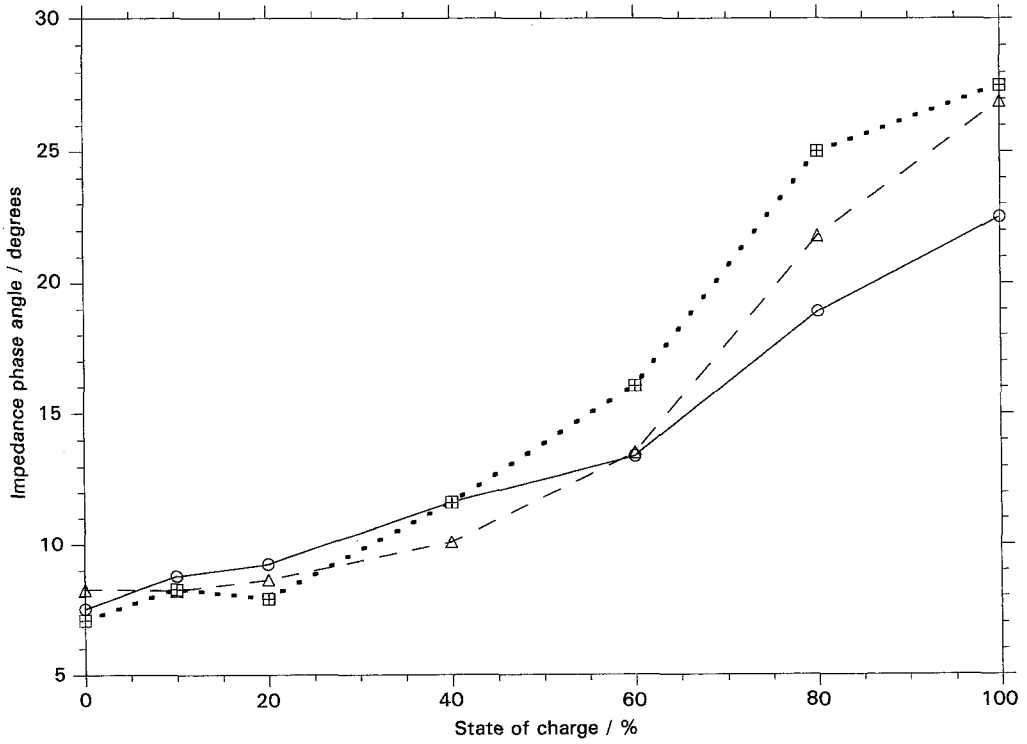

Fig. 8. Effect of state of charge on impedance phase angle at various frequencies for battery E1. The phase angle increases with increase in state of charge. Frequency: (——) 0.9, (– – –) 2.1 and (· · ·) 5.9 Hz.

Table 3. Inductive circuit parameter values for various batteries

Battery	*E1*	*E1*	*M3*	*M6*	*M6*	*N7*	*N7*	*N8*
SOC/%	0	20	20	0	20	0	10	0
$R/(\Omega)$	1.33	1.22	1.86	1.69	1.31	0.933	1.33	1.11
$L/\mu H$	0.526	0.619	0.455	0.428	0.482	0.650	0.607	0.589

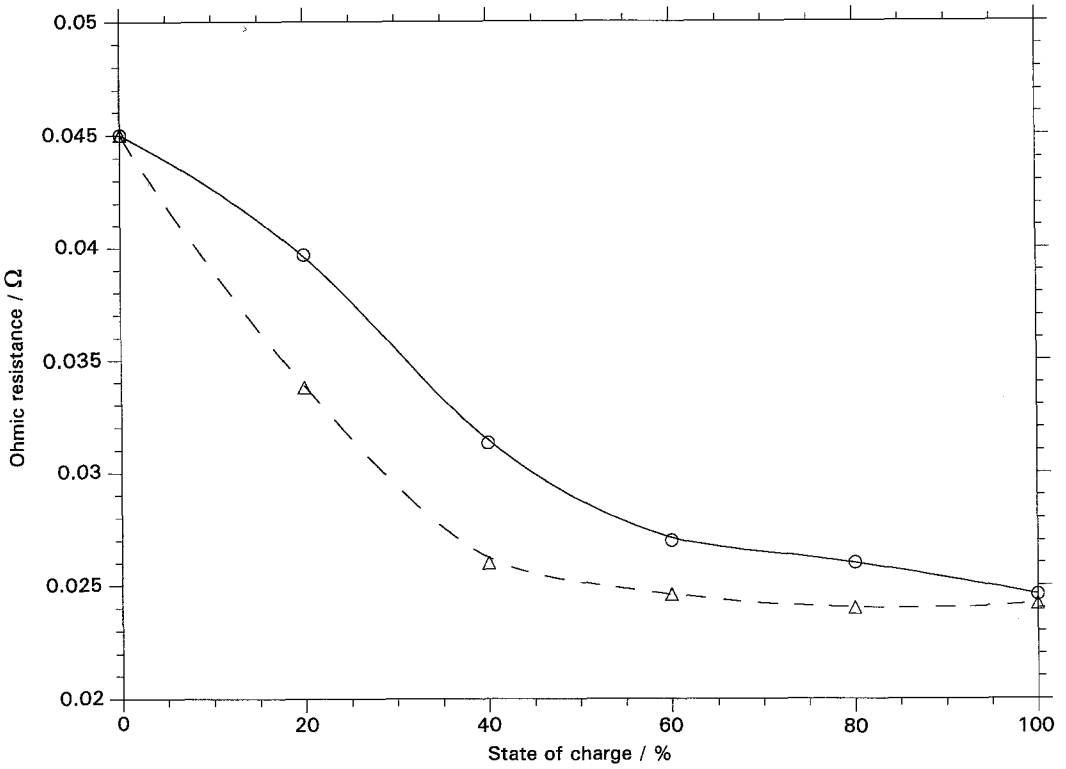

Fig. 9. Effect of state of charge on ohmic resistance R_Ω for batteries N7 (○) and N8 (△). R_Ω decreases with increase in state of charge, especially in the 0–40% range.

both by the geometry and state of charge of the battery.

The values of the circuit parameters $R_\Omega(Q_1(R_tQ_2))$ with and without the inductive data are shown in Table 5. The (RL) values for the inductive portion have already been listed in Table 3. It is clear that fitting the data without the inductive points leads to nearly the same values for the circuit parameters as those obtained with the inductive points. Due to this, the inductive points in the data for all the cells were deleted prior to equivalent circuit fitting.

Table 4. Upper frequencies limit for noninductive behaviour

SOC/%	*Frequency (Hz) above which inductive behaviour is observed*				
	M3	*M6*	*N7*	*N8*	*E1*
0	3982	2510	631	631	1584
10	—	—	631	—	1000
20	3162	1584	631	631	631
40	998	794	501	501	631
60	794	794	501	501	501
80	794	794	501	501	501
100	794	631	501	501	501

Figure 1 shows the results of the fit (Nyquist plot) for battery N7 at 0% state of charge. The semicircle is depressed at high frequencies. The quality of fit is good. Tables 6–10 show the equivalent circuit parameter values for all the batteries at various states of charge. The ohmic resistance decreased with increase in state of charge. Figure 9 shows this for batteries N7 and N8. The charge transfer resistance increased with state of charge. Figure 10 shows the increase in R_t with state of charge for batteries N7 and N8. This increase in R_t with state of charge may be due to depletion of discharged active material, leading to unavailability of active centres for charge transfer. The nonideal double layer capacitance Y_1 increased with state of charge as expected for batteries N7 and N8 (Fig. 11).

All the cases discussed so far yielded a nonideal Warburg diffusion element in the low frequency region. Figure 12 shows the Nyquist plot for battery E1 at 80% state of charge in the frequency range 0.002–631 Hz. The low frequency data points bend over towards the real axis, indicating a diffusion layer of finite length. This was modelled by a finite length diffusion element O. Table 11 gives the values of the circuit parameters for the data in which the

Table 5. Effect of inductance on equivalent circuit parameter values

*Nature**	*Battery*	*SOC*/%	R_Ω/Ω	Y_1	n_1	R_t/Ω	Y_2	n_2
L	E1	0	0.0751	0.143	0.595	0.031	11.1	0.307
			0.0885	0.188	0.711	0.020	11.8	0.316
L	M3	20	0.132	2.29	0.235	0.132	12.2	0.349
			0.163	1.02	0.484	0.058	14.3	0.321
L	M6	0	0.136	1.59	0.33	0.26	30.1	0.61
			0.150	1.20	0.42	0.20	24.1	0.52
L	M6	20	0.100	2.65	0.306	0.125	16.7	0.40
			0.115	1.37	0.476	0.070	16.7	0.357
L	N7	0	0.039	0.164	0.746	0.0066	43.3	0.256
			0.045	0.380	0.924	0.0045	50.9	0.316
L	N7	10	0.041	1.70	0.53	0.024	65.8	0.364
			0.047	1.47	0.66	0.018	64.4	0.358
L	N8	0	0.043	0.58	0.67	0.011	53.2	0.318
			0.045	0.41	0.89	0.006	53.1	0.319

* *L* corresponds to fit with inductive data points.

Table 6. Equivalent circuit parameters for Battery M3 for the circuit $R_\Omega(Q_1)(R_tQ_2)$)

SOC/%	R_Ω/Ω	Y_1	n_1	R_t/Ω	Y_2	n_2
0	0.2095	0.34	0.570	0.069	9.0	0.267
20	0.1630	1.02	0.484	0.058	14.3	0.321
40	0.1130	0.33	0.780	0.018	18.5	0.344
60	0.0890	0.57	0.757	0.017	17.9	0.384
80	0.0742	2.38	0.571	0.045	21.2	0.496
100	0.0680	2.76	0.549	0.071	26.5	0.623

Table 7. Equivalent circuit parameters for Battery M6 for the circuit $R_\Omega(Q_1)(R_tQ_2)$)

SOC/%	R_Ω/Ω	Y_1	n_1	R_t/Ω	Y_2	n_2
0	0.150	1.20	0.418	0.197	24.1	0.530
20	0.115	1.37	0.476	0.070	16.7	0.357
40	0.075	1.00	0.647	0.026	20.3	0.404
60	0.062	0.82	0.732	0.017	19.3	0.402
80	0.048	4.92	0.476	0.067	27.7	0.625
100	0.044	2.61	0.609	0.059	30.5	0.646

Table 8. Equivalent circuit parameters for Battery N7 for the circuit $R_\Omega(Q_1)(R_tQ_2)$)

SOC/%	R_Ω/Ω	Y_1	n_1	R_t/Ω	Y_2	n_2
0	0.045	0.38	0.924	0.0045	50.9	0.316
10	0.047	1.47	0.659	0.0181	64.4	0.358
20	0.040	1.95	0.776	0.0074	38.4	0.274
40	0.031	0.32	0.974	0.0060	54.0	0.361
60	0.027	1.58	0.768	0.0159	53.4	0.651
80	0.026	3.48	0.661	0.0350	38.0	0.680
100	0.025	4.43	0.639	0.0610	11.5	0.587

Table 9. Equivalent circuit parameters for Battery N8 for the circuit $R_\Omega(Q_1)(R_tQ_2)$)

SOC/%	R_Ω/Ω	Y_1	n_1	R_t/Ω	Y_2	n_2
0	0.045	0.41	0.894	0.006	53.1	0.319
20	0.034	0.29	0.959	0.005	58.7	0.363
40	0.026	1.82	0.711	0.018	80.0	0.523
60	0.025	2.48	0.698	0.029	44.0	0.635
80	0.024	3.86	0.635	0.046	32.8	0.669
100	0.024	4.49	0.639	0.073	18.7	0.627

Table 10. Equivalent circuit parameters for Battery E1 for the circuit $R_\Omega(Q_1)(R_tQ_2)$)

SOC/%	R_Ω/Ω	Y_1	n_1	R_t/Ω	Y_2	n_2
0	0.089	0.188	0.711	0.020	11.8	0.316
10	0.052	0.100	0.918	0.009	15.0	0.250
20	0.046	0.144	0.924	0.005	18.6	0.278
40	0.030	0.652	0.821	0.020	25.7	0.494
60	0.028	1.213	0.750	0.038	27.4	0.510
80	0.027	1.156	0.810	0.058	18.7	0.504
100	0.026	1.800	0.740	0.082	12.2	0.440

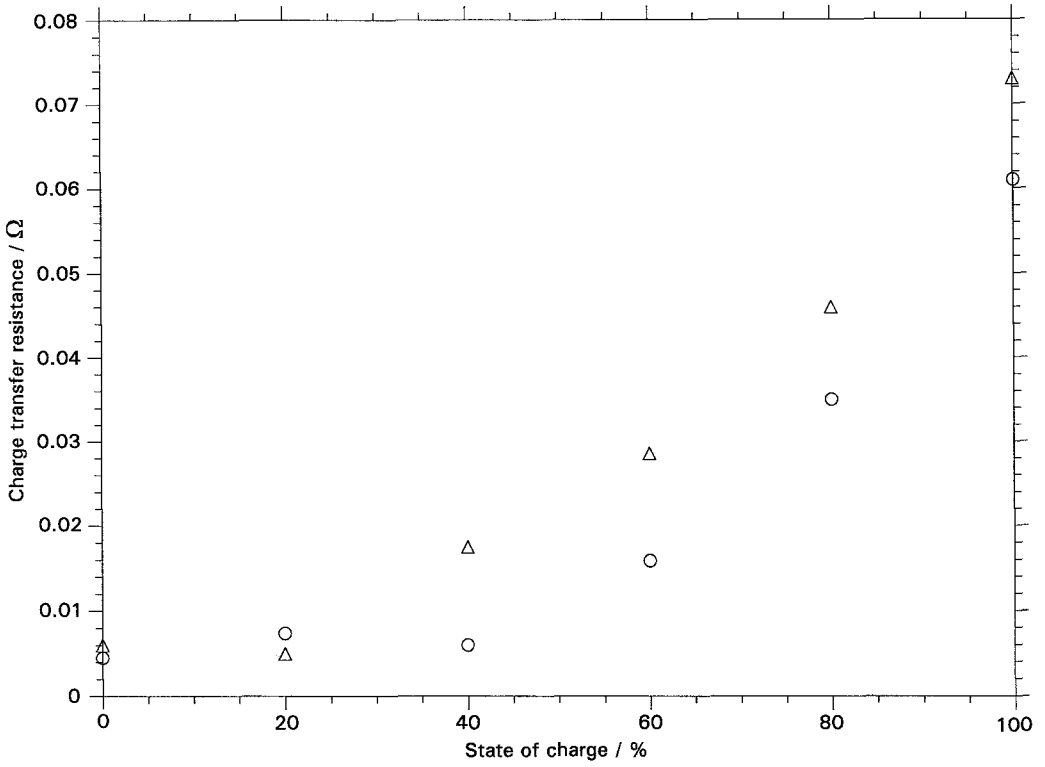

Fig. 10. Effect of state of charge on charge transfer resistance R_t for batteries N7 (O) and N8 (Δ). R_t increases with state of charge.

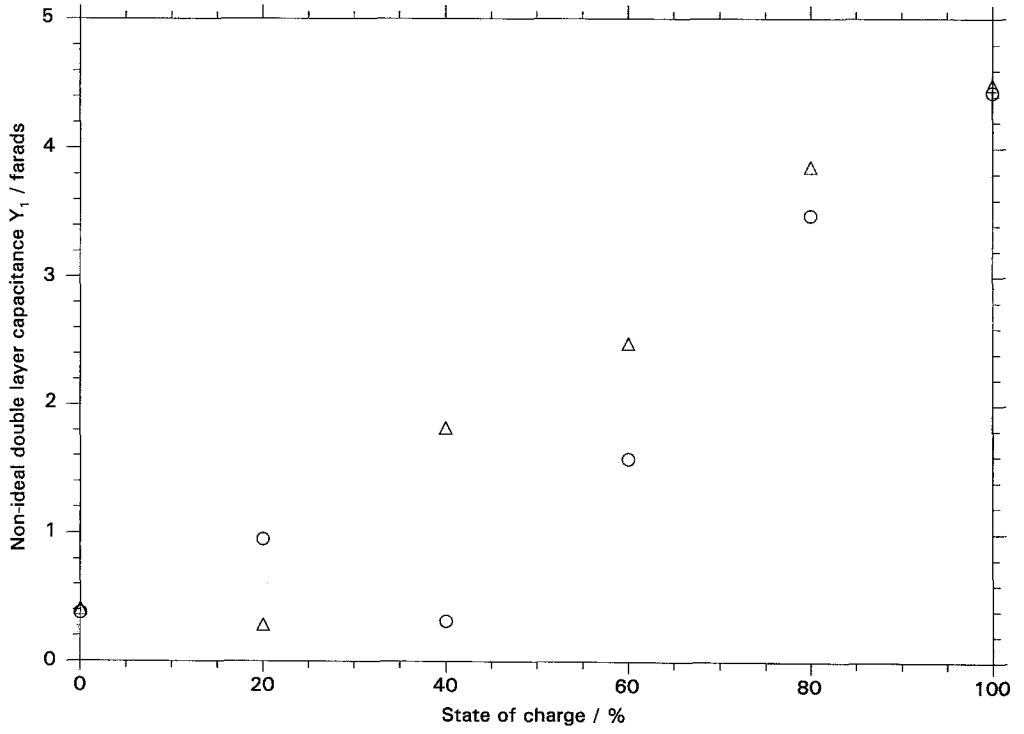

Fig. 11. Effect of state of charge on Y_1, the nonideal double layer capacitance for batteries N7 (O) and N8 (Δ).

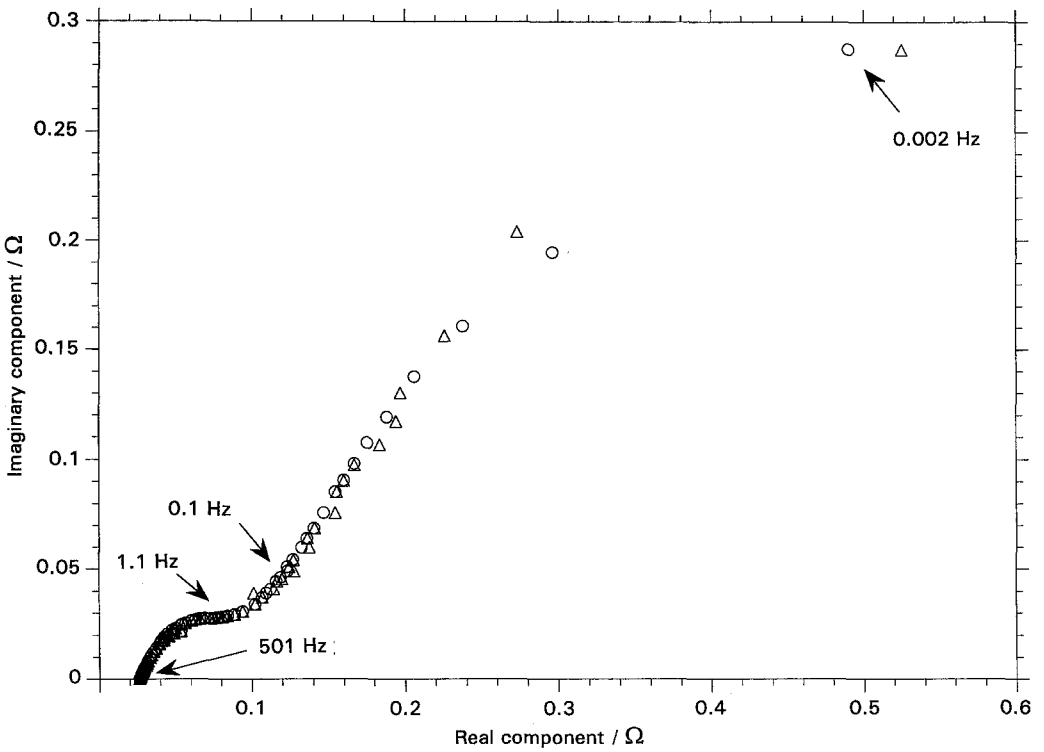

Fig. 12. Nyquist plot for finite diffusion at low frequency for battery E1 at 80% SOC. Fitting was done by using a finite diffusion element O instead of Warburg element. (○) Measurement; (△) simulation.

Table 11. Equivalent circuit parameters for the circuit (RQ(RO))

Battery	*SOC*/%	R_Ω/Ω	Y_1	n_1	R_t/Ω	$O(Y_2)$	$O(B)$
E1	60	0.0276	1.51	0.705	0.041	29.5	5.75
E1	80	0.027	1.23	0.786	0.059	18.8	13.07
M3	80	0.075	3.00	0.527	0.051	21.4	8.48

finite diffusion element was used. To test the validity of this fit, the lowest three frequency points that correspond to finite length diffusion were deleted and the data was fitted with the modified Randles' circuit. The only difference between the modified Randles' circuit and the circuit with the finite diffusion element is the substitution of the CPE Q_2 with the finite diffusion element O. The values of the circuit parameters (other than those for O and Q_2) were quite close to each other, as seen by comparison with corresponding values in Tables 6 and 10.

Conclusions

Alternating current impedance spectroscopy measurements were done on sealed lead acid batteries. The dependence of state of charge on ϕ, C_S and C_p was determined. A modified Randle's equivalent circuit using constant phase elements to represent the double layer and Warburg impedance was used and the data was fitted to the circuit. The dependence of the state of charge on the circuit parameters was determined. A finite diffusion element O was used to fit the low frequency data points bending over towards the real axis.

The following conclusions were drawn:

(i) The imaginary component passed through a minimum as a function of the state of charge. Hence the state of charge could not be determined.

(ii) The parameters ϕ, C_s and C_p were very sensitive to the state of charge at low frequency (~0.006–0.9 Hz).

(iii) A complete tabulation of the above parameters at various frequencies as a function of the state of charge enabled the determination of the state of charge of the cell, since a monotonically increasing or decreasing relationship was obtained at certain frequencies.

(iv) A modified Randles' circuit with constant phase elements fit the data well. The following results were obtained from the equivalent circuit analysis: (a) the ohmic resistance decreased with increase in state of charge; (b) the charge transfer resistance increased with increase in state of charge; and (c) the nonideal double layer capacitance increased with increase in state of charge.

References

[1] P. Casson, N. A. Hampson and M. J. Willars, *J. Electroanal. Chem.* **97** (1979) 21.
[2] N. A. Hampson, S. Kelly and K. Peters, *J. Appl. Electrochem.* **11** (1981) 751.
[3] S. Kelly, N. A. Hampson and K. Peters, *ibid.* **11** (1981) 765.
[4] J. R. Driscoll and S. Szpak, *J. Power Sources* **16** (1985) 285.
[5] J. Jindra, M. Musilova, J. Mrha and A. A. Taganova, *ibid.* **37** (1992) 403.
[6] M. Hughes, R. T. Barton, S. A. G. R. Karunathilaka and N. A. Hampson, *J. Appl. Electrochem.* **16** (1986) 555.

[7] R. T. Barton and P. J. Mitchell, *J. Power Sources* **27** (1989) 287.
[8] M. L. Gopikanth and S. Sathyanarayana, *J. Appl. Electrochem.* **9** (1979) 369.
[9] B. A. Boukamp, 'Equivalent Circuit Users Manual', 2nd edn, report: CT88/265/128, University of Twente, The Netherlands (May 1989).
[10] V. V. Viswanathan, A. J. Salkind, J. J. Kelley and J. B. Ockerman, *J. Appl. Electrochem.* Part I, this issue.
[11] M. Keddam, Z. Stoynov and T. Takenouti, *J. Appl. Electrochem.* **7** (1977) 539.